

Stability boundaries, percolation threshold, and two-phase coexistence for polydisperse fluids of adhesive colloidal particles

Riccardo Fantoni,^{a)} Domenico Gazzillo,^{b)} and Achille Giacometti^{c)}

Istituto Nazionale per la Fisica della Materia and Dipartimento di Chimica Fisica, Università di Venezia, S. Marta DD 2137, I-30123 Venezia, Italy

(Received 17 September 2004; accepted 20 October 2004; published online 28 December 2004)

We study the polydisperse Baxter model of sticky hard spheres (SHS) in the modified mean spherical approximation (mMSA). This closure is known to be the zero-order approximation C0 of the Percus-Yevick closure in a density expansion. The simplicity of the closure allows a full analytical study of the model. In particular we study stability boundaries, the percolation threshold, and the gas-liquid coexistence curves. Various possible subcases of the model are treated in details. Although the detailed behavior depends upon the particularly chosen case, we find that, in general, polydispersity inhibits instabilities, increases the extent of the nonpercolating phase, and diminishes the size of the gas-liquid coexistence region. We also consider the first-order improvement of the mMSA (C0) closure (C1) and compare the percolation and gas-liquid boundaries for the one-component system with recent Monte Carlo simulations. Our results provide a qualitative understanding of the effect of polydispersity on SHS models and are expected to shed new light on the applicability of SHS models for colloidal mixtures. © 2005 American Institute of Physics. [DOI: 10.1063/1.1831275]

I. INTRODUCTION

In sterically stabilized colloidal mixtures, particles are coated with polymer brushes to prevent irreversible flocculation due to van der Waals attraction.¹ If the solvent is a moderate one, a lowering of the temperature yields very strong attraction with a range much less than the typical colloidal size. In microemulsions of polydispersed spherical water droplets each coated by a monolayer of sodium di-2-ethylhexylsulfosuccinate dispersed in a continuum of oil, the droplets interact with each other via a hard core plus a short range attractive potential, the strength of which increases with temperature.² For these systems, a very useful theoretical model is the sticky hard sphere (SHS) model proposed by Baxter³ long time ago for atomic liquids. In the original Baxter solution^{3,4} the one-component Ornstein-Zernike (OZ) integral equation was analytically solved within the Percus-Yevick (PY) approximation. Successive extension to mixtures,⁵ however, proved to be a formidable task in view of the fact that a large [infinite (Ref. 6)] number of coupled quadratic equations ought to be solved numerically in order to have a complete understanding of both thermodynamics and structure of the model. This is the reason why, to the best of our knowledge, only binary mixtures have been explicitly discussed so far in this framework.⁵ Moreover it has been proven by Stell⁷ that sticky spheres of equal diameter in the Baxter limit are not thermodynamically stable and size polydispersity can be expected to restore thermodynamic stability.

Motivated by this scenario, it was recently proposed⁸ a

simpler approximation [modified mean spherical approximation (mMSA) closure] having the advantage that also the multicomponent case could be worked out analytically.^{9,10} Further analysis and comparison with both Monte Carlo (MC) and PY results^{8,11,12} in the one-component case, have shown that the mMSA closure for Baxter model is a reliable one up to experimentally significant densities. The price to pay for this simplification is that only the energy equation of state gives rise to a critical behavior, the other two routes yielding either a noncritical behavior (compressibility), or a diverging equation of state (virial).

In this work we pursue this investigation by studying the multicomponent version of the model proposed in Ref. 8, and analyzing various consequences. We first solve the multicomponent version of Baxter model within the mMSA closure, and show that the solution is equivalent to the one derived in Ref. 9 for a companion SHS model. The solution, derived in terms of an auxiliary function called Baxter factor correlation, turns out to be formally similar to that derived with the PY closure. However, and this is the crux of the matter, the matrix function representing the stickiness parameters is unconstrained, unlike the PY counterpart. In order to make further progress and derive the multicomponent energy equation of state, a further assumption is necessary on the matrix representing the stickiness parameters. As discussed previously (see Ref. 9 for details) a remarkable simplification occurs when the general element of this matrix has the form of a sum of dyads (i.e., it is dyadic). In these cases the necessary matrix inversion can be carried out analytically and all measurable quantities can then be computed. Physically, this reduction to a dyadic form amounts to assume a relation among polydispersity in size and polydispersity in stickiness, that is on the adhesion forces. In addition to the two cases

^{a)}Electronic mail: rfantoni@unive.it

^{b)}Electronic mail: gazzillo@unive.it

^{c)}Electronic mail: achille@unive.it

proposed in Ref. 9 (denoted as cases I and II in the following) and that proposed in Ref. 13 (case IV), we shall consider two further cases. The first one (case III) is a physically motivated variant of case I, whereas the second one (case V) has its main justification in the simplifying features occurring when one attempts to go beyond the mMSA closure with a density perturbative approach (to first order this will be called C1, as in Ref. 8, for reasons which will become apparent in the rest of the paper).

The main results of our analysis are the following. We derive the instability curves in three of the considered cases (cases I–III) within the mMSA approximation and analyze the effect of polydispersity in some detail. In order to test the reliability of the mMSA approximation, we also consider the first-order correction C1 in the one-component case and compare with the PY result.

Next we consider the effect of polydispersity on the percolation threshold. This is an interesting phenomenon on its own right and has attracted considerable attention recently,^{11,12,14–16} being a paradigmatic example of flocculation instability. In particular, recent Monte Carlo simulations^{11,12} on monodisperse (one-component) spheres with sticky adhesion have clearly tested the performance of analytical calculations based on the PY approximation.^{15,16} We then study the percolation transition as a function of polydispersity in all above mentioned cases within mMSA. Again we can discriminate the effect of polydispersity on the percolation line, and also compare it with the first-order correction C1, the PY approximation, and MC simulations in the one-component case.

Next we consider phase equilibrium. A major obstacle to the analysis of phase transition in polydisperse systems is posed by the fact that, in principle, one has to deal with a large (infinite) number of integral nonlinear equations corresponding to the coexistence conditions among various phases. In this model, however, as it also occurs in other simpler models such as hard spheres (HS),¹⁷ van der Waals fluids¹⁸ and in more complex cases such as factorizable hard-sphere Yukawa potentials,^{19,20} the task can be carried out in full detail in view of the fact that the (excess) free energy depends upon only a finite number of moments of the size distribution function. In the particular case of two-phase coexistence, we derive the cloud and shadow curves of all cases in the mMSA approximation. We compare the results with those derived earlier for a polydisperse van der Waals fluid,¹⁷ and discuss analogies and differences in this respect. Finally we compare the results of the mMSA one-component case with the first-order correction, the PY approximation, and the results of MC simulations.

The plan of the paper is as follows. In Sec. II we define the multicomponent SHS model, give the solution for Baxter factor correlation function in the mMSA (C0) approximation,

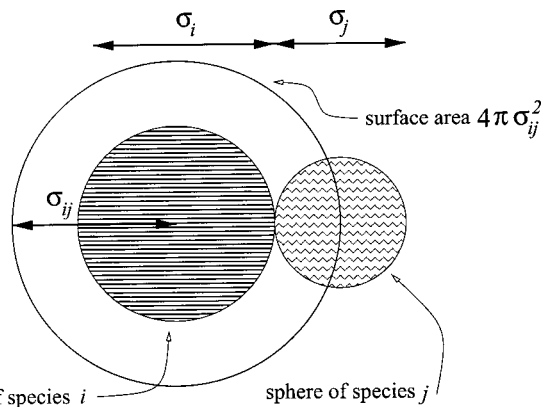


FIG. 1. Schematic diagram showing the area of the contact surface between a particle of species i and a particle of species j .

and define the various cases of polydispersion models taken under exam; in Sec. III we give the solution for Baxter factor correlation function in the C1 approximation and show how case V is particularly suitable to study the polydisperse system analytically; in Sec. IV we analytically derive the instability boundaries; in Sec. V we find analytically the percolation thresholds; in Sec. VI we derive numerically the two-phase coexistence curves; in Sec. VII we lay down our conclusions and further developments.

II. BAXTER MODEL AND MODIFIED MSA SOLUTION

In Baxter model of SHS1, one starts adding to the HS potential a square-well tail with²¹

$$\phi_{ij}(r) = -k_B T \ln \left(\frac{1}{12\tau_{ij}} \frac{R_{ij}}{R_{ij} - \sigma_{ij}} \right), \quad \sigma_{ij} \leq r \leq R_{ij}, \quad (1)$$

where $\sigma_{ij} = (\sigma_i + \sigma_j)/2$ (σ_i being the HS diameter of species i), $R_{ij} - \sigma_{ij}$ denotes the well width, k_B is Boltzmann constant, T the temperature, and the dimensionless parameter $\tau_{ij}^{-1} \geq 0$ measures the strength of surface adhesiveness or “stickiness” between particles of species i and j (τ_{ij} is also an unspecified increasing function of T). The sticky limit corresponds to taking $\{R_{ij}\} \rightarrow \{\sigma_{ij}\}$.

The Baxter form of the OZ integral equations for this model admits a very simple analytic solution if one uses the following mMSA:

$$c_{ij}(r) = f_{ij}(r) \quad \text{for } r \geq \sigma_{ij}, \quad (2)$$

where $c_{ij}(r)$ and $f_{ij}(r) = \exp[-\beta\phi_{ij}(r)] - 1$ are the direct correlation function and the Mayer function, respectively [$\beta = (k_B T)^{-1}$]. This can be easily inferred by using the formalism introduced in Ref. 8. As pointed out in that reference, the mMSA closure can be reckoned as a zero-order approximation in a perturbative expansion, and hence it will also be denoted as C0 henceforth. In terms of Baxter factor correlation functions $q_{ij}(r)$, its extension to mixtures reads

$$q_{ij}(r) = \begin{cases} \frac{1}{2} a_i (r - \sigma_{ij})^2 + (b_i + a_i \sigma_{ij})(r - \sigma_{ij}) + K_{ij}, & L_{ij} = (\sigma_i - \sigma_j)/2 \leq r \leq \sigma_{ij}, \\ 0, & \text{elsewhere,} \end{cases} \quad (3)$$

$$a_i = \frac{1}{\Delta} + \frac{3\xi_2\sigma_i}{\Delta^2} - \frac{12\xi_3}{\Delta}, \quad b_i = \left(\frac{1}{\Delta} - a_i \right) \frac{\sigma_i}{2}, \quad (4)$$

$$\xi_n = \frac{\pi}{6} \sum_{i=1}^p \rho_i \sigma_i^n, \quad \zeta_i = \frac{\pi}{6} \sum_{m=1}^p \rho_m \sigma_m K_{im}, \quad \Delta = 1 - \xi_3, \quad (5)$$

with p being the number of components, ρ_i the number density of species i , and

$$K_{ij}^{(\text{mMSA})} = \frac{1}{12\tau_{ij}} \sigma_{ij}^2 \equiv K_{ij}^0. \quad (6)$$

We remark that although Eqs. (3)–(5) are formally identical to their PY counterpart, this result is in fact simpler in such they differ in the quantity K_{ij} , which in the PY approximation reads²¹

$$K_{ij}^{(\text{PY})} = K_{ij}^0 y_{ij}^{(\text{PY})}(\sigma_{ij}) \equiv \frac{1}{12} \lambda_{ij} \sigma_{ij}^2, \quad (7)$$

where $y_{ij}^{(\text{PY})}(\sigma_{ij})$ is the contact value of the PY cavity function. In general, the parameters λ_{ij} can be determined only numerically by solving a set of $p(p+1)/2$ coupled quadratic equations,^{5,21} and this makes the multicomponent PY solution of limited interest from the practical viewpoint. In particular, a global analysis of the phase diagram proves to be a formidable task within the PY approximation.⁵ On the other hand, in view of the simplicity of Eq. (6) with respect to its PY counterpart Eq. (7), this is indeed possible within the mMSA (C0) approximation. The above results is, moreover, fully equivalent to a parallel but different sticky HS model (SHS3) studied by us in previous work.^{8,9} Hence, as discussed in those references, this analysis can be pursued analytically provided that K_{ij} has a dyadic form. To this aim, we consider polydisperse fluids with HS diameters distributed according to a Schulz distribution.²²

As regards stickiness, we choose to keep it either constant or related to the particle size. There are two main reasons for this. First, one expects the adhesion forces to depend upon the area of the contact surface between two particles (see Fig. 1), and hence on their sizes. Second and more practical reason is that this is a simple way of obtaining the required factorization. As the stickiness-size relation is not clearly understood, we consider five different possibilities, denoted as cases I–V henceforth. The three simplest choices are

$$\frac{1}{\tau_{ij}} = \frac{1}{\tau} \frac{\langle \sigma \rangle^2}{\sigma_{ij}^2}, \Rightarrow [K_{ij}^{(\text{mMSA})}]_{\text{case I}} = \frac{1}{12\tau} \langle \sigma \rangle^2, \quad (8)$$

$$\frac{1}{\tau_{ij}} = \frac{1}{\tau} \frac{\sigma_i \sigma_j}{\sigma_{ij}^2}, \Rightarrow [K_{ij}^{(\text{mMSA})}]_{\text{case II}} = \frac{1}{12\tau} \sigma_i \sigma_j, \quad (9)$$

$$\frac{1}{\tau_{ij}} = \frac{1}{\tau} \frac{\langle \sigma^2 \rangle}{\sigma_{ij}^2}, \Rightarrow [K_{ij}^{(\text{mMSA})}]_{\text{case III}} = \frac{1}{12\tau} \langle \sigma^2 \rangle, \quad (10)$$

where $\langle \sigma \rangle$ is the average HS diameter ($\langle F \rangle \equiv \sum_i x_i F_i$, here $x_i = \rho_i / \rho$ is the molar fraction of species i with $\rho = \sum_i \rho_i$ the total number density), and τ is assumed to depend only on the temperature, while the remaining factor in τ_{ij}^{-1} is a measure of stickiness strength and is related to the particle sizes.

The physical interpretation of these choices is the following. In case I the stickiness is assumed to be proportional to the surface contact area of two colloidal particles having average size $\langle \sigma \rangle$, whereas in case II the adhesion of each particle is linearly related to its size. Case III, finally, is a variant of case I where one considers an average stickiness rather than the stickiness of an average particle.

In all these cases the $K_{ij}^{(\text{mMSA})}$ matrix can be factorized as

$$K_{ij}^{(\text{mMSA})} = Y_i Y_j, \quad (11)$$

with Y_i having dimensions of length [$Y_i = (\sqrt{12\tau})^{-1} \langle \sigma \rangle$, $Y_i = (\sqrt{12\tau})^{-1} \sigma_i$, and $Y_i = (\sqrt{12\tau})^{-1} \langle \sigma^2 \rangle^{1/2}$ in cases I, II, and III, respectively]. Note that cases I and II have already been exploited by us in previous work.⁹

We also consider a case similar to that proposed by Tutschka and Kahl¹³ (henceforth denoted as case IV)

$$\frac{1}{\tau_{ij}} = \frac{1}{\tau}. \quad (12)$$

In this case the $K_{ij}^{(\text{mMSA})}$ matrix can be written as a sum of three factorized terms [as it can be immediately inferred by expanding the square $\sigma_{ij}^2 = (\sigma_i + \sigma_j)^2/4$] and has the interesting physical interpretation of being proportional to the area of the actual contact surface $4\pi\sigma_{ij}^2$ between particles of species i and j . Finally, and for reasons related to the C1 approximation that will be further elaborated below, we consider case V defined by the linear (rather than quadratic) dependence

$$\frac{1}{\tau_{ij}} = \frac{1}{\tau} \frac{\langle \sigma \rangle}{\sigma_{ij}}, \quad (13)$$

in this case the $K_{ij}^{(\text{mMSA})}$ parameters can be written as a sum of two factorized terms.

III. THE C1 APPROXIMATION

It was recently argued⁸ in the one-component case, that the mMSA (C0) approximation can be improved by including the next order term in the density expansion of the direct correlation function. Its extension to multicomponent mixtures reads

$$c_{ij}(r) = f_{ij}(r) \left[1 + \sum_m \rho_m \gamma_{imj}^{(1)}(r) \right], \quad r \geq \sigma_{ij}, \quad (14)$$

where

$$\begin{aligned} \gamma_{imj}^{(1)}(r) &= \int f_{im}(|\mathbf{r}-\mathbf{r}'|) f_{mj}(r') d\mathbf{r}' \\ &= \frac{2\pi}{r} \int_0^\infty ds s f_{im}(s) \int_{|r-s|}^{r+s} dt t f_{mj}(t), \end{aligned} \quad (15)$$

is the first-order coefficient in the density expansion of the partial indirect correlation functions $\gamma_{ij}(r)$. As discussed in Ref. 8, if we retain in the PY closure only the terms corresponding to the zero- and first-order expansion in density we recover the C1 approximation (14). It turns out that Baxter factor correlation function can still be cast in the form, Eqs. (3)–(5) but the K_{ij} parameters have the form

$$K_{ij}^{(C1)} = K_{ij}^0 y_{ij}^{(C1)}(\sigma_{ij}), \quad (16)$$

where the partial cavity functions at contact for this closure are

$$y_{ij}^{(C1)}(\sigma_{ij}) = 1 + \sum_m \rho_m \gamma_{imj}^{(1)}(\sigma_{ij}). \quad (17)$$

Using in Eq. (15) $f_{ij}(r) = -\theta(\sigma_{ij} - r) + \delta(r - \sigma_{ij})\sigma_{ij}/(12\tau_{ij})$, we find after some algebra the following result

$$\begin{aligned} \gamma_{imj}^{(1)}(\sigma_{ij}) = & \frac{2\pi}{\sigma_{ij}} \left\{ \frac{\sigma_{im}^2}{12\tau_{im}} \left[-\frac{1}{2}(\sigma_{mj}^2 - L_{jm}^2) + \frac{\sigma_{mj}^2}{12\tau_{mj}} \right] \right. \\ & + \frac{2}{3}\sigma_{ij}L_{mi}^3 + \frac{\sigma_{mj}^2}{12\tau_{mj}} \frac{1}{2}(L_{mi}^2 - \sigma_{mi}^2) \\ & + \frac{1}{4}(\sigma_{mj}^2 - \sigma_{ij}^2)(\sigma_{mi}^2 - L_{mi}^2) \\ & \left. + \frac{1}{3}\sigma_{ij}(\sigma_{mi}^3 - L_{mi}^3) - \frac{1}{8}(\sigma_{mi}^4 - L_{mi}^4) \right\}. \quad (18) \end{aligned}$$

Because of the presence of the factor $1/\sigma_{ij}$ in Eq. (18), $K_{ij}^{(C1)}$ cannot be expressed as a sum of factorized terms if we use any of the cases I, II, or III. Case IV, on the other hand, would be tractable, but it would yield $K_{ij}^{(C1)}$ as a sum of 14 factorized terms (proportional to $\sigma_i^n \sigma_j^m$ with $n, m = 0, 1, 2, 3$ except $n = m = 0, 3$) which is unmanageable in practice. In case V, on the other hand, a great simplification occurs and we find

$$K_{ij}^{(C1)} = k_0 + (\sigma_i + \sigma_j)k_1 + \sigma_i \sigma_j k_2, \quad (19)$$

where

$$k_0 = \eta \frac{1}{576} \frac{\langle \sigma \rangle^3 \langle \sigma^2 \rangle}{\langle \sigma^3 \rangle} \frac{1}{\tau^3}, \quad (20)$$

$$\begin{aligned} k_1 = & \frac{1}{24} \langle \sigma \rangle \frac{1}{\tau} + \eta \left(\frac{1}{576} \frac{\langle \sigma \rangle^4}{\langle \sigma^3 \rangle} \frac{1}{\tau^3} \right. \\ & \left. - \frac{1}{48} \frac{\langle \sigma \rangle^2 \langle \sigma^2 \rangle}{\langle \sigma^3 \rangle} \frac{1}{\tau^2} + \frac{1}{24} \langle \sigma \rangle \frac{1}{\tau} \right), \quad (21) \end{aligned}$$

$$k_2 = \eta \left(\frac{1}{576} \frac{\langle \sigma \rangle^3}{\langle \sigma^3 \rangle} \frac{1}{\tau^3} - \frac{1}{24} \frac{\langle \sigma \rangle^3}{\langle \sigma^3 \rangle} \frac{1}{\tau^2} + \frac{1}{8} \frac{\langle \sigma \rangle \langle \sigma^2 \rangle}{\langle \sigma^3 \rangle} \frac{1}{\tau} \right), \quad (22)$$

where $\eta = \xi_3$ is the packing fraction. The expression (19) is slightly more complicated than the $K_{ij}^{(mMSA)}$ treated with case IV, because of the k_0 term. This noteworthy feature is the main justification for the particular form of case V.

IV. PHASE INSTABILITIES

Our first task is the analysis of the phase instabilities for the polydisperse system only in the mMSA using cases I, II, and III.

The next level of approximation C1 is considerably more laborious (since the calculations for the C1 approximation

even in the simple case of case V requires determinants of n -dyadic matrices with $n > 4$) and we shall limit ourselves to the one-component case for simplicity.

A. mMSA approximation for the discrete polydisperse system

For p -component mixtures, one can define the following generalization of the Bhatia-Thornton concentration-concentration structure factor:²³⁻²⁵

$$S_{CC}(k) / \left(\prod_m x_m \right) = |\mathbf{S}(k)| \sum_{i,j=1}^p (x_i x_j)^{1/2} S_{ij}^{-1}(k), \quad (23)$$

where $|\mathbf{S}(k)|$ denotes the determinant of the matrix $\mathbf{S}(k)$ whose elements are the Ashcroft-Langreth partial structure factors.²⁶ Furthermore, the $S_{ij}^{-1}(k)$ functions are the elements of the inverse of $\mathbf{S}(k)$, which can be expressed as

$$S_{ij}^{-1}(k) = \delta_{ij} - (\rho_i \rho_j)^{1/2} \tilde{c}_{ij}(k) = \sum_m \hat{Q}_{mi}(-k) \hat{Q}_{mj}(k), \quad (24)$$

with $\tilde{c}_{ij}(k)$ three-dimensional Fourier transform of $c_{ij}(r)$, $\hat{Q}_{ij}(k) = \delta_{ij} - 2\pi(\rho_i \rho_j)^{1/2} \hat{q}_{ij}(k)$, and $\hat{q}_{ij}(k)$ being the unidimensional Fourier transform of $q_{ij}(r)$ (k is the magnitude of the exchanged wave vector, δ_{ij} the Kronecker delta).

Phase instability corresponds to the divergence of the long wavelength limit $S_{CC}(k=0)$, which is related to the concentration fluctuations. Taking into account the relations

$$\sum_{i,j} (x_i x_j)^{1/2} S_{ij}^{-1}(0) = \sum_i x_i a_i^2 = (\rho k_B T K_T)^{-1} = \left(\frac{\partial \beta P}{\partial \rho} \right)_T, \quad (25)$$

$$|\mathbf{S}(0)| = |\mathbf{I} - \mathbf{C}(0)|^{-1} = |\hat{\mathbf{Q}}(0)|^{-2}, \quad (26)$$

[where K_T is the isothermal compressibility, \mathbf{I} the unit matrix of order p , and \mathbf{C} has elements $(\rho_i \rho_j)^{1/2} \tilde{c}_{ij}(k)$], $S_{CC}(k=0)$ can be reexpressed as

$$\frac{S_{CC}(0)}{\prod_m x_m} = \frac{1}{|\hat{\mathbf{Q}}(0)|^2 (\rho k_B T K_T)}. \quad (27)$$

For a one-component system the divergence of K_T signals mechanical instability, associated with a gas-liquid phase transition or condensation. However, a multicomponent fluid usually becomes unstable while K_T remains finite and different from zero. In this case, it is the vanishing of $|\hat{\mathbf{Q}}(0)|$ which causes the divergence of $S_{CC}(0)$ and produces a phase instability.^{24,25} Indeed if one tries to calculate the locus of points in the phase diagram (τ, η) where $\sum_i x_i a_i^2 = 0$, using cases I, II, or III, discovers that such curves disappear (the quadratic equations in τ have a negative discriminant) as soon as we switch on the size polydispersity letting $\langle \sigma^2 \rangle \neq \langle \sigma \rangle^2$. We remark that the exact nature of this instability requires a more involved analysis and it will be deferred to a future work.

The computation of $|\hat{\mathbf{Q}}(0)|$, which usually becomes a formidable task with increasing p , is rather simple for the

mMSA solution of Baxter model when K_{ij} is factorized as in Eq. (11). In fact, $\hat{\mathbf{Q}}(k)$ becomes an n -dyadic (or Jacobi) matrix

$$\hat{Q}_{ij} = \delta_{ij} + \sum_{\nu=1}^n A_i^{(\nu)} B_j^{(\nu)} \quad (i, j = 1, \dots, p), \quad (28)$$

with the remarkable property that its determinant, which is of order p , turns out to be equal to a determinant of order n ($\ll p$ for polydisperse fluids).⁹ The necessary expressions are reported in Appendix A.

For factorized K_{ij} 's, one finds

$$\hat{Q}_{ij}(0) = \delta_{ij} + \frac{\pi}{6} (\rho_i \rho_j)^{1/2} \left[\frac{1}{\Delta} \sigma_j^3 + \sigma_i \frac{3}{\Delta} \left(\xi_2 \frac{1}{\Delta} \sigma_j^3 + \sigma_j^2 \right) - 12 Y_i \left(\xi_{1,1} \frac{1}{\Delta} \sigma_j^3 + \sigma_j Y_j \right) \right], \quad (29)$$

with

$$\xi_{m,n} = \frac{\pi}{6} \rho \langle \sigma^m Y^n \rangle, \quad (30)$$

($\langle \dots \rangle$) denotes a compositional average, i.e., $\langle FG \rangle \equiv \sum_i x_i F_i G_i$). Note that $\xi_{m,0} = \xi_m$.

We emphasize that the decomposition of Eq. (29) into $A_i^{(\nu)}$ and $B_j^{(\nu)}$ is not unique. However, $\hat{Q}_{ij}(0)$ of cases I and III is 3-dyadic (i.e., it contains $n=3$ dyadic terms), while $\hat{Q}_{ij}(0)$ of case II is simply 2-dyadic. As a consequence, one has to calculate at most a determinant of order 3. The general result for all three cases is

$$|\hat{\mathbf{Q}}(0)| = \frac{1}{\Delta^2} [(1 + 2\xi_3)(1 - 12\xi_{1,2}) + 36\xi_{2,1}^2]. \quad (31)$$

Physically admissible states must satisfy the inequality $|\hat{\mathbf{Q}}(0)| > 0$ (Ref. 27) and the stability boundary is reached when $|\hat{\mathbf{Q}}(0)| = 0$, which yields

$$\tau = \begin{cases} \frac{\langle \sigma \rangle^3}{\langle \sigma^3 \rangle} \eta - \left(\frac{\langle \sigma \rangle \langle \sigma^2 \rangle}{\langle \sigma^3 \rangle} \right)^2 \frac{3\eta^2}{1+2\eta} & \text{(case I),} \\ \frac{\eta(1-\eta)}{1+2\eta} & \text{(case II),} \\ \frac{\langle \sigma \rangle \langle \sigma^2 \rangle}{\langle \sigma^3 \rangle} \eta - \frac{\langle \sigma^2 \rangle^3}{\langle \sigma^3 \rangle^2} \frac{3\eta^2}{1+2\eta} & \text{(case III).} \end{cases} \quad (32)$$

If the HS diameters follow a Schulz distribution, then the stability boundary of cases I and III can be expressed as

$$\tau = \begin{cases} \eta \left(\frac{1}{M_1 M_2} - \frac{1}{M_2^2} \frac{3\eta}{1+2\eta} \right) & \text{(case I),} \\ \eta \left(\frac{1}{M_2} - \frac{M_1}{M_2^2} \frac{3\eta}{1+2\eta} \right) & \text{(case III),} \end{cases} \quad (33)$$

where $M_j = 1 + js^2$ with $s = [\langle \sigma^2 \rangle - \langle \sigma \rangle^2]^{1/2} / \langle \sigma \rangle$ measuring the degree of size polydispersity.

The fluid is stable at "temperatures" τ higher than those given by the previous equations (since $|\hat{\mathbf{Q}}(0)| > 0$). Let us now compare two mixtures with the same packing fraction η but different polydispersity degree s . As depicted in Fig. 2 at

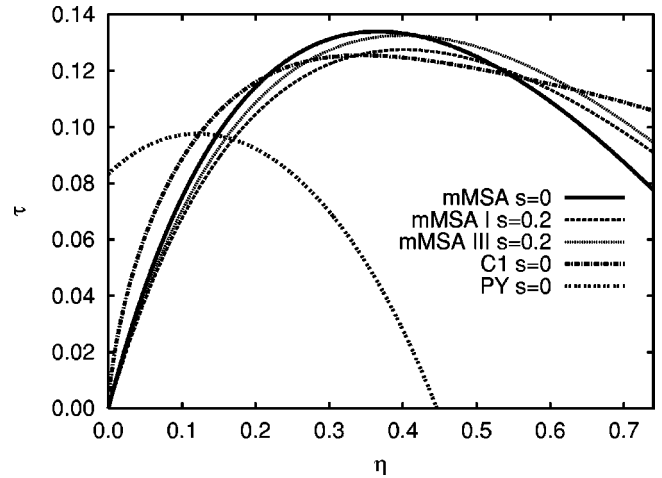


FIG. 2. Curves for the onset of phase instability (the fluid is stable above the curves shown) as obtained from the mMSA approximation for a monodisperse $s=0$ system, and for a polydisperse system with $s=0.2$, and polydispersity chosen as in cases I, II, and III [see Eq. (32)]. We also show for the one-component system the curve for the onset of mechanical instability predicted by the C1 approximation [see Eq. (34)] and the one predicted by the PY approximation [see Eq. (37)].

small η values, increasing s at fixed η lowers the stability curve of cases I and III. As shown by the left branch of the curve (the opposite trend on the right-hand side of the figure is not acceptable, since the mMSA closure can be a reasonable approximation only in the low density regime) the onset of instability occurs at lower τ . As expected, polydispersity renders the mixture more stable with respect to concentration fluctuations. Quite surprisingly, on the other hand, the stability boundary does not depend on s at fixed η in case II, and all mixtures with different polydispersity have the same stability boundary as the one-component case ($s=0$).

B. C1 approximation for the one-component system

As remarked, the C1 approximation yields rather more complex expressions and here we restrict to the one-component case. Yet, this example provides a flavor of how this approximation would work in the multicomponent case and could be compared with the result given by $|\hat{\mathbf{Q}}(0)| = 0$. For the one-component system phase instability coincides with the divergence of K_T . As from Eq. (25)

$$(\rho k_B T K_T)^{-1} = a^2 = \left[\frac{1+2\eta}{(1-\eta)^2} - \frac{1}{\tau} y^{(C1)}(\sigma) \frac{\eta}{1-\eta} \right] = 0, \quad (34)$$

where [see Eqs. (17) and (18)]

$$y^{(C1)}(\sigma) = 1 + y_1(\tau) \eta, \quad (35)$$

with

$$y_1(\tau) = \frac{5}{2} - \frac{1}{\tau} + \frac{1}{12\tau^2}. \quad (36)$$

The curve for the onset of mechanical instability is shown in Fig. 2 and compared with the PY one

$$\tau = \frac{10 - 9/(1-\eta) + 14\eta}{12(1+2\eta)}. \quad (37)$$

One clearly sees that the C1 stability boundary lowers and shifts to the left in agreement with the PY result.

V. PERCOLATION THRESHOLD

In view of the simplicity of the mMSA (C0) solution, one might expect that other quantities, besides those discussed so far, can be computed analytically. We now show that this is indeed the case. The problem we address in this section is *continuum percolation*. This problem is far from being new.²⁸ However, new activity along this line has been stirred by recent and precise Monte Carlo results for the one-component case,^{11,12} and it is then rather interesting to consider its multicomponent extension. For the sake of completeness we now recall the basic necessary formalism.¹⁴⁻¹⁶

In the sticky limit the partial Boltzmann factors read

$$e_{ij}(r) = \theta(r - \sigma_{ij}) + \frac{K_{ij}^0}{\sigma_{ij}} \delta(r - \sigma_{ij}), \quad (38)$$

where θ is the Heaviside step function and δ the Dirac delta function.

When studying percolation problems in the continuum is useful to rewrite the Boltzmann factor as the sum of two terms^{14,28} $e_{ij}(r) = e_{ij}^*(r) + e_{ij}^+(r)$, where

$$e_{ij}^*(r) = \theta(r - \sigma_{ij}), \quad (39)$$

$$e_{ij}^+(r) = \frac{K_{ij}^0}{\sigma_{ij}} \delta(r - \sigma_{ij}). \quad (40)$$

The corresponding Mayer functions will be $f_{ij}(r) = f_{ij}^*(r) + f_{ij}^+(r)$, with

$$f_{ij}^*(r) = e_{ij}^*(r) - 1, \quad (41)$$

$$f_{ij}^+(r) = e_{ij}^+(r). \quad (42)$$

The procedure to obtain equations of *connectedness* and *blocking* functions from the usual pair correlation functions and direct correlation functions is best described through the use of graphical language. If we substitute f_{ij}^* and f_{ij}^+ bonds for f_{ij} bonds in the density expansions for these functions, then the connectedness functions, which we will indicate with a cross superscript, are expressed as the sums of those terms that have at least one f_{ij}^+ bond path connecting the two root vertexes. The sums of the remaining terms in the expansions give the blocking functions.

The percolation threshold corresponds to the existence of an infinite cluster of particles and is given by the divergence of the mean cluster size^{14,28}

$$\begin{aligned} S_{\text{cluster}} &= 1 + \rho \sum_{i,j} x_i x_j \int d\mathbf{r} h_{ij}^+(r) = S_{NN}^+(k=0) \\ &\equiv \sum_{i,j} (x_i x_j)^{1/2} S_{ij}^+(k=0), \end{aligned} \quad (43)$$

where $h_{ij}^+(r)$ is the pair connectedness function (related to the joint probability of finding a particle of species i and a particle of species j at a distance r and that these two particles are connected) and

$$S_{ij}^+(k) \equiv \delta_{ij} + (\rho_i \rho_j)^{1/2} \tilde{h}_{ij}^+(k). \quad (44)$$

Since $h_{ij}^+(r)$ is related to the so called direct connectedness function $c_{ij}^+(r)$ through an OZ equation, one can use Baxter formalism again, introducing a factor function $q_{ij}^+(r)$. If we now define $\hat{Q}_{+,ij}(k) = \delta_{ij} - 2\pi(\rho_i \rho_j)^{1/2} \hat{q}_{ij}^+(k)$, then it results that

$$S_{ij}^+(k) = \sum_m \hat{Q}_{+,im}^{-1}(k) \hat{Q}_{+,jm}^{-1}(-k) \quad (45)$$

and thus

$$S_{\text{cluster}} = \sum_m s_m^2(0), \quad (46)$$

where

$$s_m(0) = \sum_i \sqrt{x_i} \hat{Q}_{+,im}^{-1}(0). \quad (47)$$

Clearly $\hat{Q}_{+,im}^{-1}(0)$ diverges to infinity when $|\hat{Q}_+(0)| = 0$, and this relation defines the percolation threshold.

Another interesting and related quantity is the average coordination number

$$\bar{Z} = 4\pi\rho \sum_{i,j} x_i x_j \int_0^{\sigma_{ij}} h_{ij}^+(r) r^2 dr. \quad (48)$$

A. mMSA approximation

The mMSA closure for $c_{ij}^+(r)$ is

$$c_{ij}^+(r) = f_{ij}^+(r) = 0, \quad r > \sigma_{ij}. \quad (49)$$

On the other hand when $r \leq \sigma_{ij}$ we have $e_{ij}^*(r) = 0$ and $f_{ij}^+(r) = e_{ij}(r)$, so we must have exactly

$$\begin{aligned} h_{ij}^+(r) &= e_{ij}^*(r) y_{ij}^+(r) + f_{ij}^+(r) y_{ij}(r) \\ &= e_{ij}(r) y_{ij}(r) = \frac{K_{ij}^0}{\sigma_{ij}} y_{ij}(\sigma_{ij}) \delta(r - \sigma_{ij}) \quad r \leq \sigma_{ij}. \end{aligned} \quad (50)$$

Within the mMSA we have for the cavity function at contact⁷

$$y_{ij}(\sigma_{ij}) = 1 \quad \text{for all } i, j. \quad (51)$$

Following the same steps of Chiew and Glandt,^{15,16} we then find (see Appendix B for details)

$$q_{ij}^+(r) = K_{ij} \theta(r - L_{ij}) \theta(\sigma_{ij} - r). \quad (52)$$

From which it follows

$$\hat{Q}_{+,ij}(0) = \delta_{ij} - 2\pi(\rho_i \rho_j)^{1/2} K_{ij} \sigma_j. \quad (53)$$

Within cases I, II, and III

$$\hat{Q}_{+,ij}(0) = \delta_{ij} + a_i^+ b_j^+, \quad (54)$$

$$a_i^+ = -2\pi\rho \sqrt{x_i} Y_i, \quad (55)$$

$$b_j^+ = \sqrt{x_j} Y_j \sigma_j. \quad (56)$$

Now from Eq. (54) follows that $\hat{Q}_{+,ij}(0)$ is a 1-dyadic form. Using the properties of dyadic matrices (see Appendix A) we then find

$$\hat{Q}_{+,ij}^{-1}(0) = \frac{1}{|\hat{Q}_+(0)|} \begin{vmatrix} \delta_{ij} & b_j^+ \\ a_i^+ & 1 + \mathbf{a}^+ \cdot \mathbf{b}^+ \end{vmatrix}, \quad (57)$$

where

$$|\hat{Q}_+(0)| = 1 + \mathbf{a}^+ \cdot \mathbf{b}^+ = 1 - 12\xi_{1,2}. \quad (58)$$

From Eq. (47) we find

$$s_m(0) = \frac{1}{|\hat{Q}_+(0)|} \left[\sqrt{x_m}(1 + \mathbf{a}^+ \cdot \mathbf{b}^+) - b_m^+ \sum_i \sqrt{x_i} a_i^+ \right], \quad (59)$$

and from Eq. (46)

$$S_{\text{cluster}} = 1 + \frac{24}{\xi_0} \frac{\xi_{1,1}\xi_{0,1}}{1 - 12\xi_{1,2}} + \frac{144}{\xi_0} \frac{\xi_{2,2}\xi_{0,1}^2}{(1 - 12\xi_{1,2})^2}. \quad (60)$$

The percolation transition occurs when

$$\tau = \begin{cases} \frac{\langle \sigma \rangle^3}{\langle \sigma^3 \rangle} \eta = \frac{1}{M_1 M_2} \eta & \text{(case I),} \\ \eta & \text{(case II),} \\ \frac{\langle \sigma \rangle \langle \sigma^2 \rangle}{\langle \sigma^3 \rangle} \eta = \frac{1}{M_2} \eta & \text{(case III).} \end{cases} \quad (61)$$

The threshold is independent of s at fixed η for case II, but lowers with increasing size polydispersity in cases I and III. The curve is simply a straight line, as a consequence of the mean-field character of the mMSA (C0) closure. The qualitative result found with cases I and III is, however, interesting. For the average coordination number we find from Eqs. (48) and (50)

$$\begin{aligned} \bar{Z} &= 4\pi\rho \sum_{i,j} x_i x_j K_{ij} \sigma_{ij} \\ &= \frac{24}{\xi_0} \xi_{1,1} \xi_{0,1} \\ &= \begin{cases} 2 \frac{\eta}{\tau} \frac{\langle \sigma \rangle^3}{\langle \sigma^3 \rangle} & \text{(case I),} \\ 2 \frac{\eta}{\tau} \frac{\langle \sigma \rangle \langle \sigma^2 \rangle}{\langle \sigma^3 \rangle} & \text{(cases II and III).} \end{cases} \end{aligned} \quad (62)$$

At the percolation transition we then find

$$\bar{Z} = \begin{cases} 2 & \text{(case I and III),} \\ 2/M_2 & \text{(case II).} \end{cases} \quad (63)$$

Using case IV $\hat{Q}_{+,ij}(0)$ turns out to be 3-dyadic; the percolation transition occurs when $|\hat{Q}_+(0)| = 0$, i.e.,

$$\begin{aligned} 1 - \frac{\eta}{\tau} - \frac{s^2(4 + 7s^2)}{8(1 + 3s^2 + 2s^4)} \left(\frac{\eta}{\tau} \right)^2 \\ + \frac{s^6}{16(1 + s^2)(1 + 2s^2)^2} \left(\frac{\eta}{\tau} \right)^3 = 0. \end{aligned} \quad (64)$$

The solution $\eta/\tau = p(s)$ such that $p(0) = 1$ is a monotonously decreasing function with

$$\lim_{s \rightarrow \infty} p(s) = 0.756431 \dots \quad (65)$$

Then with this case we find that increasing the polydispersity the nonpercolating region of the phase diagram diminishes.

With case V $\hat{Q}_{+,ij}(0)$ turns out to be 2-dyadic, and the percolation transition occurs when

$$\tau = \left(\frac{\langle \sigma \rangle \langle \sigma^2 \rangle}{\langle \sigma^3 \rangle} + \sqrt{\frac{\langle \sigma \rangle^3}{\langle \sigma^3 \rangle}} \right) \frac{\eta}{2} = \left(\frac{1}{M_2} + \sqrt{\frac{1}{M_1 M_2}} \right) \frac{\eta}{2}, \quad (66)$$

which has the physical behavior already found with cases I, II, and III.

B. C1 approximation with case V

As remarked, in case V we can work out the percolation threshold equation even within the C1 approximation. From Eq. (51) we have exactly

$$h_{ij}^+(r) = \frac{K_{ij}^0}{\sigma_{ij}} y_{ij}^{(C1)}(\sigma_{ij}) \delta(r - \sigma_{ij}), \quad r \leq \sigma_{ij}, \quad (67)$$

where $y_{ij}^{(C1)}(\sigma_{ij})$ is given by Eq. (17). For the closure condition of the direct connectedness function we find again

$$\begin{aligned} c_{ij}^+(r) &= f_{ij}^+(r) + f_{ij}^+(r) \sum_m \rho_m \gamma_{imj}^{(1)}(r) \\ &+ f_{ij}^*(r) \sum_m \rho_m \gamma_{ijm}^{(1)+}(r) = 0, \quad r > \sigma_{ij}, \end{aligned} \quad (68)$$

since $f_{ij}^+(r) = f_{ij}^*(r) = 0$ for $r > \sigma_{ij}$. To determine $q_{ij}^+(r)$ we then follow the same steps as for the mMSA case and we find

$$q_{ij}^+(r) = K_{ij}^0 y_{ij}^{(C1)}(\sigma_{ij}) \theta(r - L_{ij}) \theta(\sigma_{ij} - r). \quad (69)$$

When we insert K_{ij} from Eq. (19) into the expression for $\hat{Q}_{+,ij}(0)$ [see Eq. (53)] this becomes a 4-dyadic matrix whose determinant is

$$|\hat{Q}_+(0)| = 1 + \sum_{i=1}^6 q_i(s, \eta) / \tau^i, \quad (70)$$

where the coefficients $q_i(s, \eta)$ are given in Appendix C.

The percolation threshold is the solution of $|\hat{Q}_+(0)| = 0$. This is an algebraic equation of order 6 in τ . We can plot the correct root $\tau(\eta)$ for different values of polydispersity, as reported in Fig. 3. We see that increasing the polydispersity increases the nonpercolating phase. One can clearly observe a clear improvement from the mMSA (C0) approximation although the $\eta \rightarrow 0$ limit is still qualitatively different from the PY one-component case. It would be interesting to study if the “true” percolation threshold passes through the origin ($\eta = 0, \tau = 0$) (as occur in the C0 or C1 approximations) or has a finite limit ($\eta = 0, \tau = \tau_0$) (as it occur for monodisperse fluids in the PY approximation with $\tau_0 = 1/12$). Even if the Monte Carlo results of Refs. 11 and 12 are inconclusive in this respect, physically it is plausible to assume that at very low density the average number of bonds per particle is not sufficient to support large clusters at all and we would tend to favor the first scenario.²⁹

For the one-component system the average cluster size is

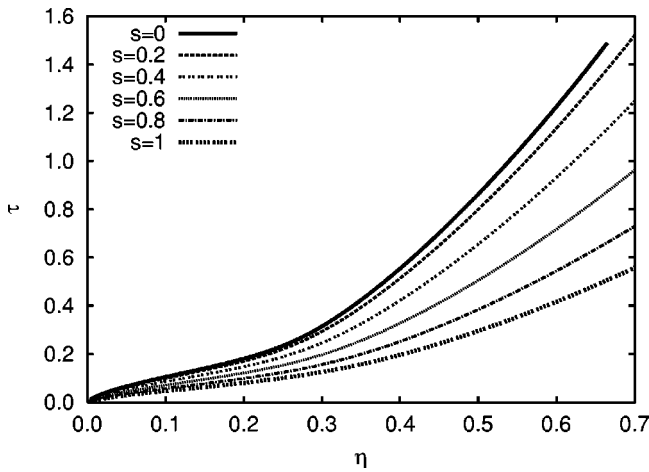


FIG. 3. Dependence of the percolation threshold, as calculated from the C1 approximation using case V (see Sec. V B), from the polydispersity.

$$\begin{aligned}
 S_{\text{cluster}} = 1 + \rho \tilde{h}^+(0) &= \frac{1}{1 - \rho \tilde{c}^+(0)} \\
 &= \frac{1}{[\hat{Q}_+(0)]^2} = \frac{1}{[1 - \eta y^{(C1)}(\sigma)/\tau]^2}.
 \end{aligned}
 \tag{71}$$

The percolation transition occurs when $\eta y^{(C1)}(\sigma) = \tau$ or

$$\eta = \frac{2(-3\tau^2 + \sqrt{3}\tau^{3/2}\sqrt{1-9\tau+30\tau^2})}{1-12\tau+30\tau^2}.
 \tag{72}$$

In Fig. 4 we compare our result for the one-component ($s=0$) system with the PY result of Chiew and Glandt¹⁵ and the Monte Carlo simulation of Miller and Frenkel.^{11,12}

The average coordination number becomes

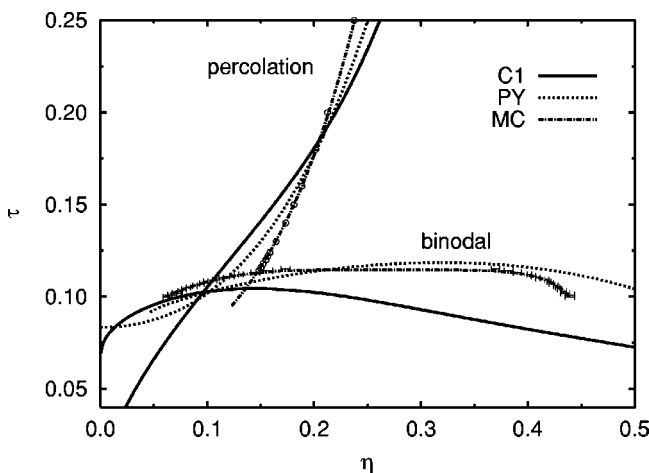


FIG. 4. Binodal curve and percolation threshold [see Eq. (73)], for a one-component system, in the C1 approximation. For comparison we also show the percolation threshold of the Percus-Yevick approximation (Ref. 15) (which exists for $\tau \geq 1/12$), the one from the Monte Carlo simulation of Miller and Frenkel (Ref. 12) (circles are the simulation results and the fit, the dot-dashed line, is only valid for $\tau \geq 0.095$), the binodal curve of the Percus-Yevick approximation (from the energy route) (Ref. 4), and the binodal curve from the Monte Carlo simulation of Miller and Frenkel (Ref. 12) (points with errorbars are the simulation results and the fit, the dot-dashed line, is merely to guide the eye).

$$\bar{Z} = 2 \frac{\eta}{\tau} y^{(C1)}(\sigma)
 \tag{73}$$

and at the percolation transition we find $\bar{Z} = 2$.

VI. PHASE EQUILIBRIUM

Phase equilibrium is another interesting aspect which can be analyzed in full details within our model. It was pointed out in Ref. 10 that the equation of state derived from the energy route for a one-component system of sticky hard spheres in the mMSA approximation is van der Waals-like. The same holds true for the system studied with the C1 approximation. It is worth stressing that the equation of state derived from the compressibility route cannot yield a van der Waals loop since from Eq. (25) $[\partial(\beta P)/\partial \rho]_T > 0$.³⁰ On the other hand the equation of state derived from the virial equation has been shown to diverge for the mMSA approximation⁸ and we anticipate that it also diverges for the C1 approximation. This is the reason why we focus our analysis on the energy route in the present work.

In this section we will find the binodal curves for the polydisperse system treated with the mMSA (C0) approximation and for the one-component system treated with the C1 approximation. The coexistence problem for a polydisperse system is, in general, a much harder task than its one-component counterpart, since it involves the solution of a large (infinite) number of integral nonlinear equations. But we will see that since our excess free energy is expressed in terms of a finite number of moments of the size distribution function (a similar feature occurs for polydisperse van der Waals models,¹⁸ for polydisperse HS (Ref. 17) and for Yukawa-like potentials^{19,20}) the coexistence problem can be simplified and becomes numerically solvable through a simple Newton-Raphson algorithm [see Eqs. (79)–(81)]. The necessary formalism to this aim can be found in a recent review,¹⁷ and we will briefly recall it next.

A. From a discrete to a continuous polydisperse mixture

Consider a mixture made of p components labeled $i = 1, \dots, p$, containing $N^{(0)}$ particles and with density $\rho^{(0)}$, which separates, at a certain temperature τ , into m daughter phases, where each phase, labeled $\alpha = 1, \dots, m$, has a number of particles $N^{(\alpha)}$ and density $\rho^{(\alpha)}$. Let the molar fraction of the particles of species i of phase α be $x_i^{(\alpha)}$, $\alpha=0$ corresponding to the parent phase. At equilibrium the following set of constraints must be fulfilled: (i) volume conservation, (ii) conservation of the total number of particles of each species, (iii) equilibrium condition for the pressures $P^{(\alpha)}(\tau, \rho^{(\alpha)}, \{x_i^{(\alpha)}\})$, and (iv) equilibrium condition for the chemical potentials $\mu_i^{(\alpha)}(\tau, \rho^{(\alpha)}, \{x_i^{(\alpha)}\})$. This set of constraints form a closed set of equations (see Appendix D for details) for the $(2+p)m$ unknowns $\rho^{(\alpha)}$, $x_i^{(\alpha)} = N^{(\alpha)}/N^{(0)}$, and $x_i^{(\alpha)}$ with $i=1, \dots, p$ and $\alpha=1, \dots, m$. Extension to the polydisperse case with an infinite number of components is achieved by switching from the discrete index variable i to the continuous variable σ using the following replacement rule:

$$x_i \rightarrow F(\sigma) d\sigma, \quad (74)$$

where $F(\sigma)d\sigma$ is the fraction of particles with diameter in the interval $(\sigma, \sigma+d\sigma)$. The function $F(\sigma)$ will be called *molar fraction density function* or more simply size distribution function. Note that, due to this replacement rule, we also have

$$P^{(\alpha)}(\tau, \rho^{(\alpha)}, \{x_i^{(\alpha)}\}) \rightarrow P^{(\alpha)}(\tau, \rho^{(\alpha)}; [F^{(\alpha)}]), \quad (75)$$

$$\mu_i^{(\alpha)}(\tau, \rho^{(\alpha)}, \{x_i^{(\alpha)}\}) \rightarrow \mu^{(\alpha)}(\sigma, \tau, \rho^{(\alpha)}; [F^{(\alpha)}]), \quad (76)$$

i.e., the thermodynamic quantities become functionals of the size distribution function and the equilibrium conditions (ii)–(iv) has to be satisfied for all values of the continuous variable σ . The phase coexistence problem that now consists in solving the constraints (i)–(iv) for the unknowns $\rho^{(\alpha)}$, $x^{(\alpha)}$, and $F^{(\alpha)}(\sigma)$ for $\alpha=1, \dots, m$, turns out to be a rather formidable task hardly solvable from a numerical point of view. Fortunately, as outlined in the following section, for our model a remarkable simplification occurs.

B. Truncatable excess free energy

As is described in the following section, the excess free energy of our system is *truncatable*: it is only a function of the three moments ξ_i , $i=1,2,3$ of the size distribution function [see Eq. (86) for cases I, II, III, IV, and V treated with mMSA, and Eq. (100) for case V treated with C1]. So we have the following simplification

$$P^{(\alpha)}(\tau, \rho^{(\alpha)}; [F^{(\alpha)}]) \rightarrow P^{(\alpha)}(\tau, \rho^{(\alpha)}; \{\xi_i^{(\alpha)}\}), \quad (77)$$

$$\mu^{(\alpha)}(\sigma, \tau, \rho^{(\alpha)}; [F^{(\alpha)}]) \rightarrow \mu^{(\alpha)}(\sigma, \tau, \rho^{(\alpha)}; \{\xi_i^{(\alpha)}\}), \quad (78)$$

where $\{\xi_i^{(\alpha)}\}$ is a short-hand notation for $\xi_1^{(\alpha)}, \xi_2^{(\alpha)}, \xi_3^{(\alpha)}$. It turns out that the two-phase ($m=2$) coexistence problem, the one in which we are interested (we are thus concentrating on the high temperature portion of the phase diagram), reduces to the solution of the following eight equations in the eight unknowns $\rho^{(1)}$, $\rho^{(2)}$, $\{\xi_i^{(1)}\}$, and $\{\xi_i^{(2)}\}$,

$$\xi_i^{(\alpha)} = \frac{\pi}{6} \rho^{(\alpha)} \int Q^{(\alpha)}(\sigma, \tau, \rho^{(0)}, \rho^{(1)}, \rho^{(2)}; \{\xi_i^{(1)}\}, \{\xi_i^{(2)}\}) \times F^{(0)}(\sigma) \sigma^i d\sigma, \quad i=1,2,3 \quad \alpha=1,2, \quad (79)$$

$$1 = \int Q^{(\alpha)}(\sigma, \tau, \rho^{(0)}, \rho^{(1)}, \rho^{(2)}; \{\xi_i^{(1)}\}, \{\xi_i^{(2)}\}) F^{(0)}(\sigma) d\sigma, \quad (80)$$

$$\alpha=1 \text{ or } 2, \quad (80)$$

$$P^{(1)}(\tau, \rho^{(1)}; \{\xi_i^{(1)}\}) = P^{(2)}(\tau, \rho^{(2)}; \{\xi_i^{(2)}\}), \quad (81)$$

with

$$\rho^{(\alpha)} Q^{(\alpha)} = \rho^{(0)} \frac{(\rho^{(1)} - \rho^{(2)})(1 - \delta_{1\alpha} + \delta_{1\alpha} e^{\beta \Delta \mu^{\text{exc}}})}{(\rho^{(1)} - \rho^{(0)}) + (\rho^{(0)} - \rho^{(2)}) e^{\beta \Delta \mu^{\text{exc}}}}, \quad (82)$$

and

$$\Delta \mu^{\text{exc}} = \mu^{\text{exc}(2)}(\sigma, \tau, \rho^{(2)}; [F^{(2)}]) - \mu^{\text{exc}(1)}(\sigma, \tau, \rho^{(1)}; [F^{(1)}]), \quad (83)$$

where we indicate with the superscript exc the excess part (over the ideal) of the chemical potential. For a complete derivation of Eqs. (79)–(81) see Appendix D.

C. Thermodynamic properties

In order to obtain the equation of state of our model Eq. (1) from the energy route, one exploits the following exact result (if $\tau_{ij} = \tau/\epsilon_{ij}$ with the ϵ_{ij} independent of τ):

$$\begin{aligned} \frac{\partial(\beta A^{\text{exc}}/N)}{\partial \tau} &= 2\pi\rho \sum_{i,j} x_i x_j \int \frac{\partial[\beta \phi_{ij}(r)]}{\partial \tau} g_{ij}(r) r^2 dr \\ &= 2\pi\rho \sum_{i,j} x_i x_j \int_{\sigma_{ij}}^{R_{ij}} \frac{1}{\tau} e_{ij}(r) y_{ij}(r) r^2 dr \\ &= 2\pi\rho \sum_{i,j} x_i x_j \frac{1}{\tau} \int_{\sigma_{ij}}^{R_{ij}} \frac{1}{12\tau_{ij}} \frac{R_{ij}}{R_{ij} - \sigma_{ij}} y_{ij}(r) r^2 dr. \end{aligned}$$

Upon taking the sticky limit we find

$$\frac{\partial(\beta A^{\text{exc}}/N)}{\partial \tau} = \frac{\eta}{\langle \sigma^3 \rangle} \frac{1}{\tau} \sum_{i,j} x_i x_j \frac{1}{\tau_{ij}} \sigma_{ij}^3 y_{ij}(\sigma_{ij}). \quad (84)$$

1. mMSA approximation

Within the mMSA approximation the partial cavity functions at contact are all equal to 1 so from Eq. (84), after integration over τ from $\tau = \infty$ (hard sphere case), we find

$$\frac{\beta(A_{\text{SHS}}^{\text{exc}} - A_{\text{HS}}^{\text{exc}})}{N} \xi_0 = \begin{cases} -\frac{1}{\tau} \frac{\xi_1^3}{\xi_0} & \text{(case I),} \\ -\frac{1}{\tau} \xi_2 \xi_1 & \text{(cases II and III),} \\ -\frac{1}{\tau} \frac{1}{4} (3\xi_1 \xi_2 + \xi_0 \xi_3) & \text{(case IV),} \\ -\frac{1}{\tau} \frac{1}{2} \left(\xi_1 \xi_2 + \frac{\xi_1^3}{\xi_0} \right) & \text{(case V).} \end{cases} \quad (85)$$

The pressure can be found, from $\beta P/\rho = \eta \partial(\beta A/N)/\partial \eta$

$$\begin{aligned} \frac{\pi}{6} \beta [P_{\text{SHS}}(\tau, \rho; \{\xi_i\}) - P_{\text{HS}}(\tau, \rho; \{\xi_i\})] \\ = \frac{\beta(A_{\text{SHS}}^{\text{exc}} - A_{\text{HS}}^{\text{exc}})}{N} \xi_0, \end{aligned} \quad (86)$$

where for P_{HS} we use an equation due to Boublík, Mansoori, Carnahan, Starling, and Leland (Refs. 31 and 32) which reduces to the Carnahan-Starling one when $s=0$,

$$\begin{aligned} & \frac{\pi}{6} \beta P_{\text{HS}}(\tau, \rho; \{\xi_i\}) \\ &= Z_{\text{HS}} \xi_0 = \frac{\xi_0}{1-\xi_3} + 3 \frac{\xi_1 \xi_2}{(1-\xi_3)^2} + 3 \frac{\xi_2^3}{(1-\xi_3)^3} \\ & \quad - \frac{\xi_3 \xi_2^3}{(1-\xi_3)^3} = \xi_0 \left\{ \frac{1}{1-\eta} + \frac{3\eta}{(1-\eta)^2} \frac{1}{M_2} \right. \\ & \quad \left. + \left[\frac{3\eta^2}{(1-\eta)^3} - \frac{\eta^3}{(1-\eta)^3} \right] \frac{M_1}{M_2^2} \right\}. \end{aligned} \quad (87)$$

The excess free energy of the polydisperse hard sphere system is obtained integrating $(Z_{\text{HS}}-1)/\eta$ over η , from $\eta=0$, and recalling that the excess free energy is zero when $\eta=0$. We then find³³

$$\begin{aligned} \frac{\beta A_{\text{HS}}^{\text{exc}}}{N} &= \frac{\eta}{(1-\eta)^2} \frac{M_1}{M_2^2} + \frac{3\eta}{1-\eta} \frac{1}{M_2} + \left[\frac{M_1}{M_2^2} - 1 \right] \ln(1-\eta) \\ &= \frac{\xi_2^3}{\xi_0 \xi_3 (1-\xi_3)^2} + 3 \frac{\xi_1 \xi_2}{\xi_0 (1-\xi_3)} \\ & \quad + \left(\frac{\xi_2^3}{\xi_0 \xi_3^2} - 1 \right) \ln(1-\xi_3). \end{aligned} \quad (88)$$

Note that both $A_{\text{HS}}^{\text{exc}}$ and $A_{\text{HS}}^{\text{exc}}$ depend upon only a finite number of moments ξ_ν , and this is the crucial feature for the feasibility of the phase equilibrium, as remarked.

For the chemical potential $\beta \mu_i = \partial(\beta A/V)/\partial \rho_i$ we find after some algebra

$$\begin{aligned} & \beta \mu^{\text{exc}}(\sigma, \tau, \rho; \{\xi_i\}) \\ &= (\mu_{\text{HS}}^{[0]} + \Delta \mu^{[0]}) + (\mu_{\text{HS}}^{[1]} + \Delta \mu^{[1]}) \sigma \\ & \quad + (\mu_{\text{HS}}^{[2]} + \Delta \mu^{[2]}) \sigma^2 + (\mu_{\text{HS}}^{[3]} + \Delta \mu^{[3]}) \sigma^3, \end{aligned} \quad (89)$$

where

$$\mu_{\text{HS}}^{[0]} = -\ln(1-\xi_3), \quad (90)$$

$$\mu_{\text{HS}}^{[1]} = 3\xi_2/(1-\xi_3), \quad (91)$$

$$\begin{aligned} \mu_{\text{HS}}^{[2]} &= \left(3 \frac{\xi_2^2}{\xi_3} \right) \ln(1-\xi_3) \\ & \quad + 3\xi_1/(1-\xi_3) + \left(3 \frac{\xi_2^2}{\xi_3} \right) / (1-\xi_3)^2, \end{aligned} \quad (92)$$

$$\begin{aligned} \mu_{\text{HS}}^{[3]} &= \left(-2 \frac{\xi_2^3}{\xi_3^2} \right) \ln(1-\xi_3) + \left(\xi_0 - \frac{\xi_2^3}{\xi_3^2} \right) / (1-\xi_3) \\ & \quad + \left(3\xi_1\xi_2 - \frac{\xi_2^3}{\xi_3^2} \right) / (1-\xi_3)^2 + \left(2 \frac{\xi_2^3}{\xi_3^2} \right) / (1-\xi_3)^3. \end{aligned} \quad (93)$$

and

$$\Delta \mu^{[0]} = \begin{cases} \frac{1}{\tau} \frac{\xi_1^3}{\xi_0^2} & \text{(case I),} \\ 0 & \text{(cases II and III),} \\ -\frac{1}{\tau} \frac{\xi_3}{4} & \text{(case IV),} \\ \frac{1}{\tau} \frac{\xi_1^3}{2\xi_0^2} & \text{(case V),} \end{cases} \quad (94)$$

$$\Delta \mu^{[1]} = \begin{cases} -\frac{1}{\tau} \frac{3\xi_1^2}{\xi_0} & \text{(case I),} \\ -\frac{1}{\tau} \xi_2 & \text{(cases II and III),} \\ -\frac{1}{\tau} \frac{3\xi_2}{4} & \text{(case IV),} \\ -\frac{1}{\tau} \frac{1}{2} \left(\xi_2 + \frac{3\xi_1^2}{\xi_0} \right) & \text{(case V),} \end{cases} \quad (95)$$

$$\Delta \mu^{[2]} = \begin{cases} 0 & \text{(case I),} \\ -\frac{1}{\tau} \xi_1 & \text{(cases II and III),} \\ -\frac{1}{\tau} \frac{3\xi_1}{4} & \text{(case IV),} \\ -\frac{1}{\tau} \frac{\xi_1}{2} & \text{(case V),} \end{cases} \quad (96)$$

$$\Delta \mu^{[3]} = \begin{cases} 0 & \text{(case I),} \\ 0 & \text{(cases II and III),} \\ -\frac{1}{\tau} \frac{\xi_0}{4} & \text{(case IV),} \\ 0 & \text{(case V).} \end{cases} \quad (97)$$

It is noteworthy that if we retain in the expression (87) for P_{HS} , only the first term, then our case IV coincides with the van der Waals model of Bellier-Castella *et al.*¹⁸ with $n=1$, $l=0$, upon identifying 4τ with the temperature used by these authors.

2. C1 approximation with case V

In analogy with what we have done before, we now consider the C1 approximation for case V. Using Eq. (17) into Eq. (84)

$$\begin{aligned} \frac{\partial(\beta A^{\text{exc}}/N)}{\partial \tau} &= 12 \frac{\eta}{\tau} \left[k_0 \frac{\langle \sigma \rangle}{\langle \sigma^3 \rangle} + k_1 \left(\frac{\langle \sigma^2 \rangle + \langle \sigma \rangle^2}{\langle \sigma^3 \rangle} \right) \right. \\ & \quad \left. + k_2 \frac{\langle \sigma^2 \rangle \langle \sigma \rangle}{\langle \sigma^3 \rangle} \right]. \end{aligned} \quad (98)$$

Integrating from $\tau=\infty$ we find

TABLE I. For the one-component system, we compare the critical parameters obtained from the mMSA, C1, and PY (Ref. 4) approximations with the ones from the Monte Carlo simulation of Miller and Frenkel (Ref. 12).

	τ_c	η_c	$(Z_{\text{SHS}})_c$
mMSA	0.0943	0.13	0.36
C1	0.1043	0.14	0.37
PY	0.1185	0.32	0.32
MC	0.1133	0.27	---

$$\frac{\beta(A_{\text{SHS}}^{\text{exc}} - A_{\text{HS}}^{\text{exc}})}{N} = -\frac{\eta}{2} \frac{1}{\tau} \left(\frac{\langle \sigma \rangle^3}{\langle \sigma^3 \rangle} + \frac{\langle \sigma \rangle \langle \sigma^2 \rangle}{\langle \sigma^3 \rangle} \right) + \frac{\eta^2}{2} \left[-\frac{1}{\tau} \left(\frac{\langle \sigma \rangle \langle \sigma^2 \rangle}{\langle \sigma^3 \rangle} + \frac{\langle \sigma \rangle^3}{\langle \sigma^3 \rangle} + 3 \frac{\langle \sigma \rangle^2 \langle \sigma^2 \rangle}{\langle \sigma^3 \rangle^2} \right) + \frac{1}{\tau^2} \left(\frac{1}{4} \frac{\langle \sigma \rangle^2 \langle \sigma^2 \rangle^2}{\langle \sigma^3 \rangle^2} + \frac{3}{4} \frac{\langle \sigma \rangle^4 \langle \sigma^2 \rangle}{\langle \sigma^3 \rangle^2} \right) - \frac{1}{\tau^3} \left(\frac{1}{72} \frac{\langle \sigma \rangle^6}{\langle \sigma^3 \rangle^2} + \frac{1}{24} \frac{\langle \sigma \rangle^4 \langle \sigma^2 \rangle}{\langle \sigma^3 \rangle^2} \right) \right]. \quad (99)$$

For this case we limit ourselves to study the coexistence problem for the one-component system. In Table I we compare the critical parameters obtained through the energy route for the mMSA, C1, PY approximations and MC simulation, for the one-component system.

Note that, as already pointed out in Ref. 8, a density expansion of $y(\sigma)$ within the PY approximation gives to zero order the $y(\sigma)$ of the mMSA approximation and to first order the $y(\sigma)$ of the C1 approximation (as should be expected comparing the density expansions of the closures corresponding to these approximations). So at low densities Z_{SHS} from mMSA, C1, and PY should be comparable. From Table I we see that the true critical parameters are between the PY and the C1 ones.

In Fig. 4 we depict the binodal curve obtained from the C1 approximation for the one-component system and we compare it with the PY binodal curve (obtained from the energy route) Ref. 4 and the one resulting from the MC simulation of Miller and Frenkel.¹² Remarkably, the gas-liquid coexistence curve predicted by C1 lies closer to the MC data than the one predicted by PY on the gas branch and further on the liquid branch.

D. Numerical results

In this section we describe the numerical results obtained from the solution of Eqs. (79)–(81) for the SHS in the mMSA, through a Newton-Raphson algorithm.

We first determined the *cloud* and *shadow* curves by solving Eqs. (79)–(81) for the particular case in which we set $\rho^{(0)} = \rho^{(1)}$ so that $F^{(1)}(\sigma) = F^{(0)}(\sigma)$. The cloud curve $\rho_c(\tau)$ is such that the solutions $\rho^{(1)}(\tau)$, $\rho^{(2)}(\tau)$ of the full coexistence problem given by Eqs. (79)–(81), for a fixed $\rho^{(0)}$ (the coexistence or binodal curves), have the property that for a certain temperature τ_0 , $\rho^{(1)}(\tau_0) = \rho_c(\tau_0) = \rho^{(0)}$, i.e., the density of phase 1 ends on the cloud curve. The shadow curve is the set of points $\rho_s(\tau)$ in equilibrium with the corresponding

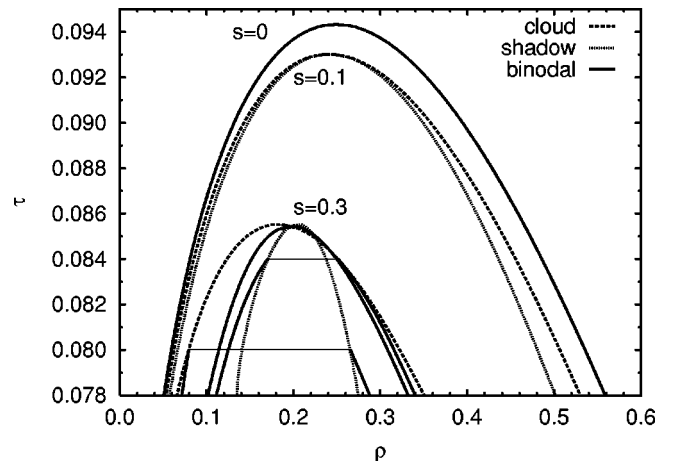


FIG. 5. Cloud and shadow curves for case I in the mMSA at two values of polydispersity: $s=0.1$ and $s=0.3$. For the case $s=0.3$ we also show three coexistence curves (continuous lines) obtained setting $\rho^{(0)}=0.08$, $\rho^{(0)}=0.25$, and $\rho^{(0)}=0.197 \approx \rho_{\text{cr}}$. For comparison the binodal of the monodisperse ($s=0$) system has also been included.

cloud curve, i.e., $\rho^{(2)}(\tau_0) = \rho_s(\tau_0)$, the density of phase 2 ends on the shadow curve. The interception between the cloud and the corresponding shadow curve gives the critical point $(\tau_{\text{cr}}, \rho_{\text{cr}})$: when $\rho^{(0)} = \rho_{\text{cr}}$ the two solutions $\rho^{(1)}(\tau)$, $\rho^{(2)}(\tau)$ meet at the critical point.

In order to find the cloud and shadow curves we choose as the parent distribution $F^{(0)}(\sigma)$ a Schulz distribution with $\langle \sigma \rangle = 1$, and the initial conditions, for the Newton-Raphson algorithm, in the high temperature τ_* and low polydispersity s_* region. Our starting conditions for the solution are

$$\rho^{(\alpha)} = \rho_{\text{oc}}^{(\alpha)}, \quad (100)$$

$$\xi_1^{(\alpha)} = \frac{\pi}{6} \rho^{(\alpha)}, \quad (101)$$

$$\xi_2^{(\alpha)} = \frac{\pi}{6} \rho^{(\alpha)} (1 + s_*^2), \quad (102)$$

$$\xi_3^{(\alpha)} = \frac{\pi}{6} \rho^{(\alpha)} (1 + s_*^2) (1 + 2s_*^2), \quad (103)$$

for $\alpha=1,2$, where $\rho_{\text{oc}}^{(1)}$ and $\rho_{\text{oc}}^{(2)}$ are the coexistence densities at a temperature τ_* for the one-component system. Once the cloud and shadow curves are determined we proceed to find the coexistence curves for a given mother density.

In Fig. 5 we depict the cloud and shadow curves obtained with our case I for two representative values of polydispersity, $s=0.1$ and $s=0.3$. For comparison the coexistence curve of the one-component system ($s=0$) is also reported. As polydispersity increases, the critical point moves to lower densities and lower temperatures ($\tau_{\text{cr}} \approx 0.094$, $\rho_{\text{cr}} \approx 0.249$ at $s=0$, $\tau_{\text{cr}} \approx 0.093$, $\rho_{\text{cr}} \approx 0.24$ at $s=0.1$, and $\tau_{\text{cr}} \approx 0.085$, $\rho_{\text{cr}} \approx 0.197$ at $s=0.3$). Let us now fix $s=0.3$, a value corresponding to a moderate polydispersity. Again in Fig. 5 we depict three coexistence curves upon changing the mother density $\rho^{(0)}=0.08$, $\rho^{(0)}=0.25$, and $\rho^{(0)}=0.197 \approx \rho_{\text{cr}}$.

All these curves closely resemble the corresponding ones obtained for the polydisperse van der Waals model,¹⁸ in

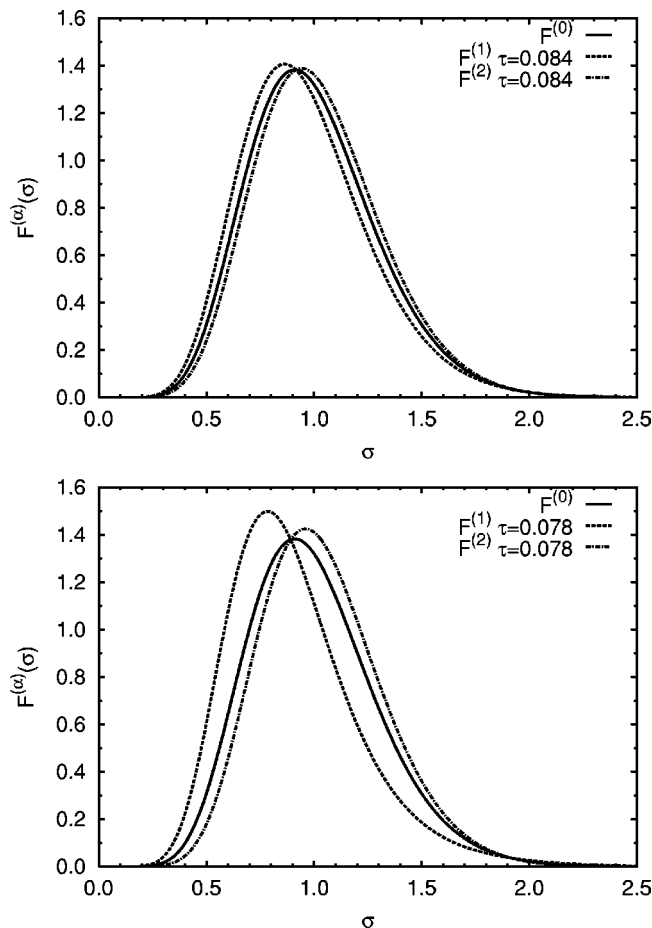


FIG. 6. Evolution of the size distribution of the coexisting phases $F^{(1)}(\sigma)$ and $F^{(2)}(\sigma)$, with temperature along the critical binodal of Fig. 5 ($s=0.3$, $\rho^{(0)}=0.197 \approx \rho_{cr}$). For comparison also the parent Schulz distribution is shown (continuous line).

agreement with previous results. In Fig. 6 we show how the two daughter distribution functions (at $s=0.3$ and $\rho^{(0)} = \rho_{cr}$) differ from the parent Schulz distribution (a process usually called *fractionation*), for two different values of temperature $\tau=0.084$ and $\tau=0.078$.

Next we consider differences in the critical behavior with respect to change in the case. In Fig. 7 we show the cloud and shadow curves obtained using cases I, IV, and V at $s=0.3$. While for cases I and V the critical point is displaced at lower temperature and lower density respect to the monodisperse system, the critical point of case IV is displaced at higher temperatures and lower density. The cloud curves of cases II and III have a low density branch that does not meet the high density one as soon as $s>0$; moreover, the cloud curve does not meet the corresponding shadow curve, so there is no critical point. We are not aware of similar features in other polydisperse models, although this is of course to be expected in other cases as well.

VII. CONCLUSIONS

In this work we have performed an extensive analysis of the phase diagram for Baxter SHS model in the presence of polydispersity. In spite of its simplicity, this model has been proven to be extremely useful in the theoretical characteriza-

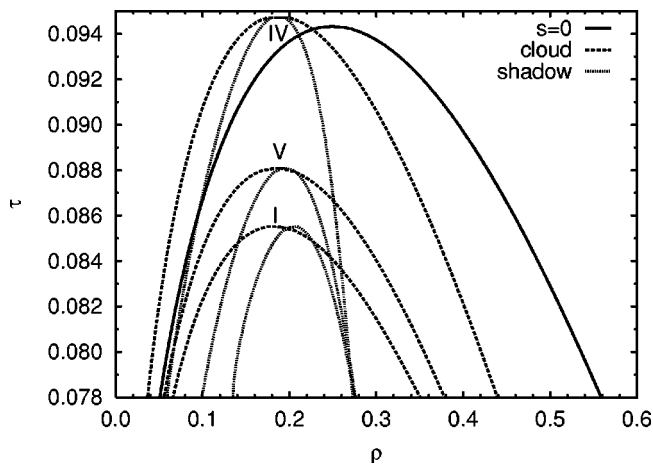


FIG. 7. Cloud and shadow curves for cases I, IV, and V in the mMSA at $s=0.3$. For comparison the binodal of the monodisperse ($s=0$) system has also been included (continuous line).

tion of sterically stabilized colloids. These systems are, however, affected by intrinsic polydispersity in some of their physical properties (size, species, etc.) and hence the effect of polydispersity on the corresponding theoretical models cannot be overlooked and is then a rather interesting point to address. As only formal manipulations⁵ can be carried out for the multicomponent Baxter SHS model within the PY approximation, we have resorted to a simpler closure mMSA to which the PY closure reduces in the limit of zero density and that was recently shown⁸ to reproduce rather precisely many of the interesting features of its PY counterpart. Our analysis has also been inspired by recent results by Miller and Frankel¹² who showed that Baxter SHS model coupled with PY closure reproduced fairly well their MC data in the one-component case. We have studied the effect of polydispersity on phase stability boundaries, the percolation phase transition, and the gas-liquid phase transition. We have considered five different cases of polydispersity. This is because there is no general agreement on the way in which adhesion forces are depending on the size of particles. Cases I and II had already been discussed in previous work by us,⁹ case III is a variant of case I, whereas a case similar to case IV had been employed by Tutschka and Kahl.¹³ Finally case V has been specifically devised to cope with approximation C1. In spite of the apparent redundancy of all these subcases, we believe that each of these examples has a reasonable interest on its own, and hence we have included them all in our discussion.

We studied the instability boundaries and the two-phase coexistence problem of polydisperse SHS system in the mMSA (C0). The next level of approximation C1 would still be feasible, but significantly more lengthily. We have laid down the necessary formalism in Secs. III and VI.C.2, and tested its effect on the one-component case, by comparing the results against the PY approximation and MC data. We derived the percolation threshold of the polydisperse system both within mMSA (C0) closure (for all five cases) and in the C1 approximation (using case V).

We found that the effect of polydispersity on the stability and phase boundaries slightly depends upon the chosen case, but there are general features shared by all of them: polydis-

persivity renders the mixture more stable with respect to concentration fluctuations (in the small density region, see Fig. 2) with the exception of case II for which the stability boundary is independent from the polydispersity; Eqs. (61), (64), and (66) (in the mMSA), and Eq. (70) (in the C1), describe its effect on the percolation threshold (see Figs. 4 and 3). Polydispersity increases the region of the phase diagram where we have a nonpercolating phase, with the exception of case IV, for which the opposite trend is observed, and of case II for which the percolation threshold is independent from the polydispersity; polydispersity reduces the region of the phase diagram where we have a gas-liquid coexistence for cases I and V, while the opposite trend is observed for case IV (see Fig. 7). For cases II and III we obtained cloud curves with a gap at high temperature, moreover the cloud curve does not meet the corresponding shadow curve, so there is no critical point, as soon as polydispersity is introduced.

In conclusion, the typical effect of polydispersity is to reduce the size of the unstable region, the percolating region, and the two-phase region of the phase diagram, although exceptions to this general rule have been observed for cases II, III, and IV.

For the one-component case we also compared the percolation threshold and binodal curve obtained from the C1 approximation with the results from the PY approximation^{4,15} and the results from the Monte Carlo simulation of Miller and Frenkel¹² (see Fig. 4). The percolation threshold from C1 appears to approach that from PY, but is still significantly different from the results from the Monte Carlo simulation (the zero density limit, on the other hand, appears to be more physically sound than the PY one, and this feature remains to be elucidated). The gas-liquid coexistence curve predicted by C1 is better than the one given by PY on the gas branch and worse on the liquid branch. Table I shows how the true (from the Monte Carlo simulation of Miller and Frenkel¹²) critical temperature and density for the gas-liquid coexistence should lay between the ones predicted by PY and the ones predicted by C1.

Future developments of the present work can be envisaged along the following lines: (i) as pointed out in Ref. 24 on defining $\psi_G = \Pi_m x_m / S_{CC}(0)$ and $\psi_A = \Pi_m x_m / [(\rho k_B T K_T) S_{CC}(0)]$, the condition $\psi_G > 0$ is necessary but not sufficient for the material stability of the system and the condition $\psi_A > 0$ is necessary but not sufficient for the mixed material and mechanical stability. It could happen that those two conditions are satisfied but the system is nonetheless unstable as occurs, for example, in the binary mixture stud-

ied by Chen and Forstmann.³⁴ Even though a characterization of the instability boundary in the spirit of Chen and Forstmann seems unattainable for a polydisperse system, it would be desirable, in the future, a more precise location of the instability boundaries. Moreover the way we found the instability boundaries for the polydisperse system was to start from the instability condition valid for a discrete mixture and take the limit of a continuous mixture on the instability boundaries of the discrete mixture. It would be interesting to compare our analysis with the one given by Bellier-Castella *et al.* (see Sec. IIC in Ref. 18) who take the continuous limit from the outset; (ii) all the percolation thresholds that we have calculated have a low density branch that enters the gas-liquid coexistence region. The same feature is observed for the one-component system studied through Monte Carlo simulation.^{11,12} While it is clear that continuum percolation is, strictly speaking, not a thermodynamic phase transition, one could expect, from a “dynamical” point of view, an interference between the formation of infinite clusters of particles and phase separation, and a clarification of this point would have interesting experimental applications; and (iii) the polydisperse system is expected to display, in the low temperature region, other critical points signaling the onset of $m > 2$ phase coexistence,¹⁸ and it would be interesting to study their evolution with polydispersity for our system.

ACKNOWLEDGMENT

This work was supported by the Italian MIUR (PRIN-COFIN 2004/2005).

APPENDIX A: DETERMINANT AND INVERSE OF A DYADIC MATRIX

Given the n -dyadic matrix of Eq. (28), its determinant is

$$|\hat{\mathbf{Q}}| = \begin{vmatrix} 1 + \mathbf{A}^{(1)} \cdot \mathbf{B}^{(1)} & \mathbf{A}^{(1)} \cdot \mathbf{B}^{(2)} & \dots & \mathbf{A}^{(1)} \cdot \mathbf{B}^{(n)} \\ \mathbf{A}^{(2)} \cdot \mathbf{B}^{(1)} & 1 + \mathbf{A}^{(2)} \cdot \mathbf{B}^{(2)} & \dots & \mathbf{A}^{(2)} \cdot \mathbf{B}^{(n)} \\ \vdots & \vdots & \ddots & \vdots \\ \mathbf{A}^{(n)} \cdot \mathbf{B}^{(1)} & \mathbf{A}^{(n)} \cdot \mathbf{B}^{(2)} & \dots & 1 + \mathbf{A}^{(n)} \cdot \mathbf{B}^{(n)} \end{vmatrix}. \quad (\text{A1})$$

Furthermore, any dyadic matrix $\hat{\mathbf{Q}}$ admits *analytic* inverse for any number p of components, with elements given by

$$\hat{\mathbf{Q}}_{ij}^{-1} = \frac{1}{|\hat{\mathbf{Q}}|} \begin{vmatrix} \delta_{ij} & B_j^{(1)} & B_j^{(2)} & \dots & B_j^{(n)} \\ A_i^{(1)} & 1 + \mathbf{A}^{(1)} \cdot \mathbf{B}^{(1)} & \mathbf{A}^{(1)} \cdot \mathbf{B}^{(2)} & \dots & \mathbf{A}^{(1)} \cdot \mathbf{B}^{(n)} \\ A_i^{(2)} & \mathbf{A}^{(2)} \cdot \mathbf{B}^{(1)} & 1 + \mathbf{A}^{(2)} \cdot \mathbf{B}^{(2)} & \dots & \mathbf{A}^{(2)} \cdot \mathbf{B}^{(n)} \\ \vdots & \vdots & \vdots & \ddots & \vdots \\ A_i^{(n)} & \mathbf{A}^{(n)} \cdot \mathbf{B}^{(1)} & \mathbf{A}^{(n)} \cdot \mathbf{B}^{(2)} & \dots & 1 + \mathbf{A}^{(n)} \cdot \mathbf{B}^{(n)} \end{vmatrix}. \quad (\text{A2})$$

APPENDIX B: DERIVATION OF EQ. (52)

The closure condition (49) justify the usual generalized Wiener-Hopf factorization³⁵

$$rc_{ij}^+(|r|) = -q_{ij}^+(r) + 2\pi \sum_m \rho_m \int_{L_{mi}}^{\infty} dt q_{mi}^+(t) q_{mj}^+(r+t), \quad (\text{B1})$$

$$rh_{ij}^+(|r|) = -q_{ij}^+(r) + 2\pi \sum_m \rho_m \int_{L_{im}}^{\infty} dt q_{im}^+(t)(r-t) \\ \times h_{mj}^+(|r-t|), \quad (\text{B2})$$

where $r > L_{ij}$, the prime denotes differentiation, and $q_{ij}^+(r)$ are real functions with support on $[L_{ij}, \sigma_{ij}]$ and zero everywhere else.

Let us determine $q_{ij}^+(r)$. Using the exact condition (50) in Eq. (B2) we find for $L_{ij} < r \leq \sigma_{ij}$

$$q_{ij}^+(r) = -K_{ij} \delta(|r| - \sigma_{ij}) + 2\pi \sum_m \rho_m \int_{L_{im}}^{\sigma_{im}} dt q_{im}^+(t) \\ \times (r-t) \frac{K_{mj}}{\sigma_{mj}} \delta(|r-t| - \sigma_{mj}). \quad (\text{B3})$$

The second term on the right end side is equal to $2\pi \sum_m \rho_m q_{im}^+(r - \sigma_{mj}) K_{mj}$ which is zero when $r < \sigma_{ij}$. So we simply have

$$q_{ij}^+(r) = -K_{ij} \delta(|r| - \sigma_{ij}), \quad L_{ij} < r \leq \sigma_{ij}. \quad (\text{B4})$$

Integrating this equation gives Eq. (52).

APPENDIX C: COEFFICIENTS OF EQ. (70)

The coefficients in Eq. (70) are as follows:

$$q_1(s, \eta) = -\frac{\eta(2+5\eta)(1+3s^2+2s^4)^3}{2(1+s^2)^3(1+2s^2)^4}, \quad (\text{C1})$$

$$q_2(s, \eta) = -\frac{\eta^2\{-4 + [\eta(2+\eta) - 5]s^2\}(1+3s^2+2s^4)^2}{4(1+s^2)^3(1+2s^2)^4}, \quad (\text{C2})$$

$$q_3(s, \eta) = \frac{\eta^2\{-2 + [6\eta(1+\eta) - 5]s^2 - 2s^4\}}{24(1+s^2)(1+2s^2)^3}, \quad (\text{C3})$$

$$q_4(s, \eta) = -\frac{\eta^3 s^2 [2 + 5\eta + (4 + 7\eta)s^2]}{96(1+s^2)^2(1+2s^2)^4}, \quad (\text{C4})$$

$$q_5(s, \eta) = 0, \quad (\text{C5})$$

$$q_6(s, \eta) = \frac{\eta^4 s^4}{2304(1+s^2)^3(1+2s^2)^4}. \quad (\text{C6})$$

APPENDIX D: PHASE COEXISTENCE CONDITIONS

In this Appendix we give a complete derivation of Eqs. (79)–(81) in the main text.

Consider a p -component mixture. Each species i has number density $\rho_i^{(0)} = N_i^{(0)}/V^{(0)}$, where $N_i^{(0)}$ is the number of particles of type i and $V^{(0)}$ the volume of the system.

We assume that at a certain temperature τ the system separates into m daughter phases, where each phase $\alpha = 1, \dots, m$ is characterized by a volume $V^{(\alpha)}$ and a number of particles of species i , $N_i^{(\alpha)}$.

At equilibrium the following set of constraints must be fulfilled.

(1) Volume conservation

$$V^{(0)} = \sum_{\alpha=1}^m V^{(\alpha)}; \quad (\text{D1})$$

(2) Conservation of the total number of particles of each species

$$N_i^{(0)} = \sum_{\alpha=1}^m N_i^{(\alpha)}, \quad i = 1, \dots, p, \quad (\text{D2})$$

(3) equilibrium condition for the pressures

$$P^{(\alpha)}(\tau, V^{(\alpha)}, \{N_i^{(\alpha)}\}) = P^{(\beta)}(\tau, V^{(\beta)}, \{N_i^{(\beta)}\}); \quad (\text{D3})$$

(4) equilibrium condition for the chemical potentials

$$\mu_i^{(\alpha)}(\tau, V^{(\alpha)}, \{N_i^{(\alpha)}\}) = \mu_i^{(\beta)}(\tau, V^{(\beta)}, \{N_i^{(\beta)}\}), \\ i = 1, \dots, p, \quad (\text{D4})$$

where $\{N_i^{(\alpha)}\}$ is a short-hand notation for $N_1^{(\alpha)}, \dots, N_p^{(\alpha)}$.

It is convenient to use the following set of variables: τ , $\rho^{(\alpha)} = N^{(\alpha)}/V^{(\alpha)}$, $x_i^{(\alpha)} = N_i^{(\alpha)}/N^{(\alpha)}$, $i = 1, \dots, p$ with $N^{(\alpha)} = \sum_i N_i^{(\alpha)}$. Introducing $x^{(\alpha)} = N^{(\alpha)}/N^{(0)}$ Eqs. (D1)–(D4) can be rewritten as follows:

$$\frac{1}{\rho^{(0)}} = \sum_{\alpha} \frac{1}{\rho^{(\alpha)}} x^{(\alpha)}, \quad (\text{D5})$$

$$x_i^{(0)} = \sum_{\alpha} x_i^{(\alpha)} x^{(\alpha)}, \quad (\text{D6})$$

$$P^{(\alpha)}(\tau, \rho^{(\alpha)}, \{x_i^{(\alpha)}\}) = P^{(\beta)}(\tau, \rho^{(\beta)}, \{x_i^{(\beta)}\}), \quad (\text{D7})$$

$$\mu_i^{(\alpha)}(\tau, \rho^{(\alpha)}, \{x_i^{(\alpha)}\}) = \mu_i^{(\beta)}(\tau, \rho^{(\beta)}, \{x_i^{(\beta)}\}), \quad (\text{D8})$$

with the normalization condition

$$\sum_i x_i^{(\alpha)} = 1, \quad \alpha = 1, \dots, m. \quad (\text{D9})$$

Equations (D5)–(D9) form a set of closed equations for the $(2+p)m$ unknowns $\rho^{(\alpha)}$, $x^{(\alpha)}$, $x_i^{(\alpha)}$ with $i = 1, \dots, p$ and $\alpha = 1, \dots, m$. Note that when $m = p + 1$ the densities of the various phases $\rho^{(\alpha)}$ will be independent of $\rho^{(0)}$, since relations (D7), (D8), and (D9) form a closed set of equations for the unknowns $\rho^{(\alpha)}$, $x_i^{(\alpha)}$.

In the continuous polydisperse limit ($p \rightarrow \infty$) we have to take into account the substitution rule (74). Then the thermodynamic quantities will be rewritten as in Eqs. (75) and (76), and Eqs. (D5)–(D8) become

$$\frac{1}{\rho^{(0)}} = \sum_{\alpha} \frac{1}{\rho^{(\alpha)}} x^{(\alpha)}, \quad (\text{D10})$$

$$F^{(0)}(\sigma) = \sum_{\alpha} F^{(\alpha)}(\sigma) x^{(\alpha)}, \quad (\text{D11})$$

$$P^{(\alpha)}(\tau, \rho^{(\alpha)}; [F^{(\alpha)}]) = P^{(\beta)}(\tau, \rho^{(\beta)}; [F^{(\beta)}]), \quad (\text{D12})$$

$$\mu^{(\alpha)}(\sigma, \tau, \rho^{(\alpha)}; [F^{(\alpha)}]) = \mu^{(\beta)}(\sigma, \tau, \rho^{(\beta)}; [F^{(\beta)}]), \quad (\text{D13})$$

with the normalization condition

$$\int F^{(\alpha)}(\sigma) d\sigma = 1, \quad \alpha = 1, \dots, m. \quad (\text{D14})$$

Integrating Eq. (D11) over σ and using Eq. (D14) we find

$$\sum_{\alpha} x^{(\alpha)} = 1. \quad (\text{D15})$$

The set of Eqs. (D10)–(D14) forms a closed set of equations for the unknowns $\rho^{(\alpha)}$, $x^{(\alpha)}$, and $F^{(\alpha)}(\sigma)$ with $\alpha = 1, \dots, m$. Note that, due to the substitution rule (74), sum over i becomes integration over σ and thermodynamic quantities become functionals of the distribution function. We have indicated such dependence with square brackets.

Two-phase coexistence

Let us now specialize ourselves to the two-phase ($m = 2$) coexistence. We are thus concentrating on the high temperature portion of the phase diagram, since coexistence with $m > 2$ (Gibbs phase rule does not restrict the value of m in a system of infinitely many species) is expected to occur at low temperatures. From Eqs. (D15) and (D10) we find

$$x^{(1)} = \frac{\rho^{(0)} - \rho^{(2)}}{\rho^{(1)} - \rho^{(2)}} \frac{\rho^{(1)}}{\rho^{(0)}}, \quad (\text{D16})$$

$$x^{(2)} = \frac{\rho^{(1)} - \rho^{(0)}}{\rho^{(1)} - \rho^{(2)}} \frac{\rho^{(2)}}{\rho^{(0)}}. \quad (\text{D17})$$

Note that $x^{(1)}$ and $x^{(2)}$ must be positive. So if $\rho^{(1)} < \rho^{(2)}$, then $\rho^{(0)}$ must lie between $\rho^{(1)}$ and $\rho^{(2)}$, if $\rho^{(2)} < \rho^{(1)}$, it must lie between $\rho^{(2)}$ and $\rho^{(1)}$. Substituting these expressions in Eq. (D11) we find

$$\rho^{(2)} F^{(2)} = \rho^{(0)} F^{(0)} \frac{\rho^{(1)} - \rho^{(2)}}{\rho^{(1)} - \rho^{(0)}} + \rho^{(1)} F^{(1)} \frac{\rho^{(0)} - \rho^{(2)}}{\rho^{(0)} - \rho^{(1)}}. \quad (\text{D18})$$

Next we divide the chemical potentials in their ideal and excess components $\mu = \mu^{\text{id}} + \mu^{\text{exc}}$ where

$$\beta \mu^{\text{id}(\alpha)}(\sigma, \tau, \rho^{(\alpha)}; [F^{(\alpha)}]) = \ln[\Lambda^3 \rho^{(\alpha)} F^{(\alpha)}(\sigma)], \quad (\text{D19})$$

with Λ being the de Broglie thermal wavelength. Now Eq. (D13) becomes

$$F^{(1)}(\sigma) = F^{(2)}(\sigma) \frac{\rho^{(2)}}{\rho^{(1)}} e^{\beta \Delta \mu^{\text{exc}}}, \quad (\text{D20})$$

$$\begin{aligned} \Delta \mu^{\text{exc}} = & \mu^{\text{exc}(2)}(\sigma, \tau, \rho^{(2)}; [F^{(2)}]) \\ & - \mu^{\text{exc}(1)}(\sigma, \tau, \rho^{(1)}; [F^{(1)}]). \end{aligned} \quad (\text{D21})$$

From Eqs. (D18) and (D20) we find

$$F^{(\alpha)}(\sigma) = F^{(0)}(\sigma) Q^{(\alpha)}(\sigma, \tau, \rho^{(0)}, \rho^{(1)}, \rho^{(2)}; [F^{(1)}], [F^{(2)}]), \quad (\text{D22})$$

where the $Q^{(\alpha)}$ are defined by Eq. (82).

Formally Eqs. (D18), (D20), and (D12) with $\alpha = 1$, $\beta = 2$, and (D14) with $\alpha = 1$ or 2, form a closed set of equations for the unknowns $\rho^{(1)}$, $\rho^{(2)}$, $F^{(1)}(\sigma)$, and $F^{(2)}(\sigma)$. In our case the free energy of the system [cases I, II, III, IV, and V treated with mMSA, see Eq. (85), or case V treated with C1, see Eq. (99)] is *truncatable*: it is only a function of the three moments ξ_i , $i = 1, 2, 3$ of the size distribution function F . So the problem is mapped into the solution of the eight Eqs. (79)–(81) in the eight unknowns $\rho^{(1)}$, $\rho^{(2)}$, $\xi_1^{(1)}$, $\xi_2^{(1)}$, $\xi_3^{(1)}$, $\xi_1^{(2)}$, $\xi_2^{(2)}$, and $\xi_3^{(2)}$.

¹H. Löwen, Phys. Rep. **237**, 249 (1994).

²S. H. Chen, J. Rouch, F. Sciortino, and P. Tartaglia, J. Phys.: Condens. Matter **6**, 10855 (1994).

³R. J. Baxter, J. Chem. Phys. **49**, 2770 (1968).

⁴R. O. Watts, D. Henderson, and R. J. Baxter, Adv. Chem. Phys. **21**, 421 (1971).

⁵B. Barboy and R. Tenne, Chem. Phys. **38**, 369 (1979).

⁶Strictly speaking we should distinguish between *discrete polydispersity* (multicomponent mixture with a large number of components $p \approx 10^2 - 10^3$) and a *continuous polydispersity* corresponding to $p \rightarrow \infty$ with a continuous distribution of sizes or other properties. This distinction will be specified in more details in Sec. VI.

⁷G. Stell, J. Stat. Phys. **63**, 1203 (1991).

⁸D. Gazzillo and A. Giacometti, J. Chem. Phys. **120**, 4742 (2004).

⁹D. Gazzillo and A. Giacometti, J. Chem. Phys. **113**, 9837 (2000).

¹⁰D. Gazzillo and A. Giacometti, Mol. Phys. **101**, 2171 (2003).

¹¹M. A. Miller and D. Frenkel, Phys. Rev. Lett. **90**, 135702 (2003).

¹²M. A. Miller and D. Frenkel, J. Chem. Phys. **121**, 535 (2004).

¹³C. Tutschka and G. Kahl, J. Chem. Phys. **108**, 9498 (1998).

¹⁴A. Coniglio, U. De Angelis, and A. Forlani, J. Phys. A **10**, 1123 (1977).

¹⁵Y. C. Chiew and E. D. Glandt, J. Phys. A **16**, 2599 (1983).

¹⁶Y. C. Chiew and E. D. Glandt, J. Phys. A **22**, 3969 (1989).

¹⁷P. Sollich, J. Phys.: Condens. Matter **14**, R79 (2002).

¹⁸L. Bellier-Castella, H. Xu, and M. Baus, J. Chem. Phys. **113**, 8337 (2000).

¹⁹Y. V. Kalyuzhnyi and G. Kahl, J. Chem. Phys. **119**, 7335 (2003).

²⁰Y. V. Kalyuzhnyi, G. Kahl, and P. T. Cummings, J. Chem. Phys. **120**, 10133 (2004).

²¹J. W. Perram and E. R. Smith, Chem. Phys. Lett. **35**, 138 (1975).

²²Here, for simplicity, we disregard possible complications arising from the fact that unphysically large particles are included in this analysis. These were discussed in Ref. 19.

²³A. B. Bhatia and D. E. Thornton, Phys. Rev. B **2**, 3004 (1970).

²⁴D. Gazzillo, Mol. Phys. **83**, 1171 (1994).

²⁵D. Gazzillo, Mol. Phys. **84**, 303 (1995).

²⁶N. W. Ashcroft and D. C. Langreth, Phys. Rev. **156**, 685 (1967).

²⁷B. Barboy, Chem. Phys. **11**, 357 (1975).

²⁸T. L. Hill, J. Chem. Phys. **23**, 617 (1955).

²⁹In this respect both C0 and C1 would be more precise than the PY closure and this is a remarkable feature.

³⁰Even though it may happen that one has loss of solution of $\sum_i x_i a_i^2$ for certain values of the density, as occurs for the Percus-Yevick closure (Ref. 3).

³¹T. Boublík, J. Chem. Phys. **53**, 471 (1970).

³²G. A. Mansoori, N. F. Carnahan, K. E. Starling, and T. W. Leland, Jr., J. Chem. Phys. **54**, 1523 (1971).

³³J. J. Salacuse and G. Stell, J. Chem. Phys. **77**, 3714 (1982).

³⁴X. S. Chen and F. Forstmann, J. Chem. Phys. **97**, 3696 (1992).

³⁵R. J. Baxter, J. Chem. Phys. **52**, 4559 (1970).